

Momentum and position detection in nanoelectromechanical systems beyond the Born and Markov approximations

Stefan Walter and Björn Trauzettel

Institute for Theoretical Physics and Astrophysics, University of Würzburg, D-97074 Würzburg, Germany

(Received 21 December 2010; published 7 April 2011)

We propose and analyze different schemes to probe the quantum nature of nanoelectromechanical systems (NEMS) by a tunnel junction detector. Using the Keldysh technique, we are able to investigate the dynamics of the combined system for an arbitrary ratio of $eV/\hbar\Omega$, where V is the applied bias of the tunnel junction and Ω is the eigenfrequency of the oscillator. In this sense, we go beyond the Markov approximation of previous works where these parameters were restricted to the regime $eV/\hbar\Omega \gg 1$. Furthermore, we also go beyond the Born approximation by expanding the finite frequency current noise of the tunnel junction up to fourth order in the tunneling amplitudes. Interestingly, we discover different ways to probe both position and momentum properties of NEMS. On the one hand, for a nonstationary oscillator, we find a complex finite frequency noise of the tunnel junction, concluding that a simple tunnel junction detector can probe both position- and momentum-based observables of the nonstationary oscillator. On the other hand, for a stationary oscillator, an Aharonov-Bohm-loop tunnel junction detector is needed. It still allows us to extract position and momentum information of the oscillator. For this type of detector, we analyze what happens if the energy scales eV , $\hbar\Omega$, and $k_B T_{\text{env}}$ take arbitrary values with respect to each other where T_{env} is the temperature of an external heat bath.

DOI: [10.1103/PhysRevB.83.155411](https://doi.org/10.1103/PhysRevB.83.155411)

PACS number(s): 85.85.+j, 72.70.+m, 07.50.Hp, 42.50.Lc

I. INTRODUCTION

Nanoelectromechanical systems (NEMSs) have become a promising playground for probing the quantum behavior of mesoscopic objects, theoretically as well as experimentally.^{1,2} The diverse reasons to study NEMS are their vast number of (possible) applications such as, for instance, the measurement of mass, force, and position³⁻⁷ with high precision.

Nanomechanical systems being at the boarder of classical to quantum are also being studied from a very fundamental point of view. This includes the observation, measurement, and control of quantum states of a mesoscopic mechanical continuous variable system such as a harmonic oscillator. Superconducting qubits electrically coupled to the mechanical system have been successfully used to characterize the mechanical resonator's quantum state.⁸

Making quantum effects visible in nanomechanical systems calls for ultralow temperatures and low dissipation. The goal of observing the quantum-mechanical ground state of a harmonic oscillator requires temperatures $k_B T \ll \hbar\Omega$. Recently, this goal has been achieved by using a microwave-frequency mechanical oscillator, with a frequency of $f \approx 6$ GHz which allowed cooling to the ground state with conventional cryogenic refrigeration.⁹ Further proposals of cooling a nanomechanical resonator coupled to an optical cavity have been proposed^{10,11} and experimentally implemented.^{12,13}

The theoretical treatment of NEMS widely uses a Markovian master-equation approach¹⁴⁻¹⁷ with a few exceptions, for instance, the work by Wabnig *et al.*¹⁸ and Rastelli *et al.*¹⁹ where a Keldysh perturbation theory has been employed.

Here, we also make use of the Keldysh technique because it allows us to treat the nonequilibrium system fully quantum mechanically and, furthermore, to carefully investigate the non-Markovian regime where $eV \ll \hbar\Omega$. Since we are interested in the quantum nature of the oscillator, it is important that the temperature T and the applied bias V of the tunnel junction are not much larger than the eigenfrequency Ω of

the oscillator. Otherwise, the oscillator would be heated and low-energy properties inaccessible.

The paper is organized as follows. Our key results are summarized in Sec. II. In Sec. III, we introduce the generic model. This is followed by an introduction of the formalism we use in Sec. IV with subsections focusing on the fermionic reservoir and on the oscillator dynamics. The main part of this paper is presented in Sec. V, where we discuss the calculation as well as the results for the finite frequency current noise. Finally, we conclude in Sec. VI.

II. KEY RESULTS OF THE PAPER

The motivation of our work is to study an experimentally feasible setup in which the quantum nature of NEMS can be probed by current noise measurements of a tunnel junction detector. A quantum NEMS can be described by a quantum harmonic oscillator which is a continuous variable system characterized by two noncommuting operators \hat{x} and \hat{p} . Therefore it is desirable to have a detector at hand that can measure expectation values with respect to \hat{x} -dependent observables, \hat{p} -dependent observables, as well as observables that depend on both \hat{x} and \hat{p} .

In Ref. 17, Doiron *et al.* have proposed a setup which could be used for position and momentum detection of NEMS. This setup consists of two tunnel junctions forming an Aharonov-Bohm (AB) loop. There, it is possible to tune the relative phase between the tunnel amplitudes (where one depends on \hat{x} and the other one not) via a magnetic flux penetrating the AB loop; see Fig. 1 for the schematic setup. In such a setup, the symmetrized current noise

$$S_{\text{sym}}(\omega) = \frac{1}{2} \int dt e^{i\omega t} \langle \{ \Delta \hat{I}(t), \Delta \hat{I}(0) \} \rangle \quad (1)$$

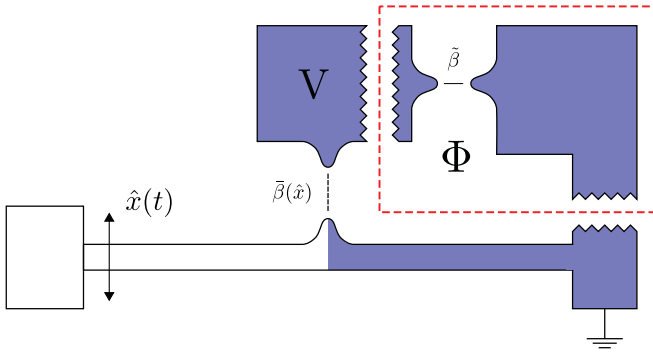


FIG. 1. (Color online) Schematic setup for the realization of a position detector that can be extended by the parts enclosed in the red dashed box to a momentum detector. The total tunnel amplitude in the case of the position detector is given as $\beta = \tilde{\beta}(\hat{x}) = t_0 + t_1 \hat{x}$ and in the case of the momentum detector as $\beta = \tilde{\beta}(\hat{x}) + \tilde{\beta} = t_0 + t_1 e^{i\eta} \hat{x}$, where the relative phase η between t_0 and t_1 can be tuned via a magnetic flux Φ penetrating the AB loop. If the oscillator is in a nonstationary state, already the parts without the elements in the red dashed box serve as a position as well as a momentum detector.

(with the current fluctuation operator $\Delta \hat{I}(t) = \hat{I}(t) - \langle \hat{I} \rangle$) of the tunnel junction detector can either contain information on the oscillator's position spectrum,

$$S_x(\omega) = \frac{1}{2} \int dt e^{i\omega t} \langle \{\hat{x}(t), \hat{x}(0)\} \rangle, \quad (2)$$

then $S_{\text{sym}}(\omega) \sim S_x(\omega)$, or the oscillator's momentum spectrum

$$S_p(\omega) = \frac{1}{2} \int dt e^{i\omega t} \langle \{\hat{p}(t), \hat{p}(0)\} \rangle, \quad (3)$$

then $S_{\text{sym}}(\omega) \sim S_p(\omega)$, see also Eq. (54) below. The current noise $S_{\text{sym}}(\omega)$ can also contain information on both the position and the momentum of the oscillator. The former case has been coined x detector and the latter case p detector. We note that $S_{\text{sym}}(\omega)$, $S_x(\omega)$, and $S_p(\omega)$ are properly defined above in Eqs. (1)–(3) for a stationary problem. In the nonstationary case, which is also the subject of discussion in this work, these quantities do not only depend on a single frequency ω but on one frequency argument and one time argument instead; see Eq. (38).

To be more specific, in this paper, we call an x detector a detector that allows us to measure expectation values of the oscillator's position operator \hat{x} , i.e., $\langle \hat{x} \rangle$, $\langle \hat{x} \hat{x} \rangle$, etc. Similarly, we call a p detector a detector that allows us to measure expectation values of \hat{p} , the oscillator's momentum operator, i.e., $\langle \hat{p} \rangle$, $\langle \hat{p} \hat{p} \rangle$, etc. In Ref. 17, switching from the x detector to the p detector is then accomplished by tuning the relative phase between the tunnel amplitudes. The main difficulty of this setup is the need of long coherence times and lengths in the AB loop to make the switching possible. Here, we show that the AB setup can be avoided. We find that the current noise of the coupled oscillator-junction system with one tunnel junction only, already can be used for momentum detection due to the complex nature of the current noise when the oscillator is in a *nonstationary* state. This is the first key result of our work, specified and intensively discussed in Sec. VB 2 below.

We further investigate the current noise stemming from a stationary oscillator up to fourth order in the tunneling

amplitudes, thereby going beyond the Born approximation. Most importantly, we extend previous results of Ref. 17 to the non-Markovian regime without any restrictions on the relative magnitude of the energy scales eV , $\hbar\Omega$, and $k_B T$. We show that peaks in the finite frequency current noise at $\omega = \pm\Omega$ (both for the x detector and the p detector) are a fourth-order effect. In the Markovian regime, the peaks in the position detector signal are always much larger than the ones in the momentum detector signal. This is different in the non-Markovian regime. There, we even find a larger signal for the momentum detector compared to the position detector, clearly demonstrating that the non-Markovian regime is the preferred regime to operate the momentum detector. The detailed understanding of the x detector and the p detector developed in this paper allows us to uniquely identify the quantum state of the oscillator by a finite frequency noise measurement. This is the second key result of our work, specified and intensively discussed in Secs. VC 4 and VC 5 below.

III. MODEL

The system we consider consists of a nanomechanical harmonic oscillator coupled to a biased tunnel junction. In Ref. 20 an experimental realization is shown, where electrons can tunnel from an atomic point contact (APC) onto a conducting oscillator. The coupled system is described by the following Hamiltonian:

$$\hat{H} = \hat{H}_{\text{osc}} + \hat{H}_{\text{res}} + \hat{H}_{\text{tun}}, \quad (4)$$

with

$$\hat{H}_{\text{osc}} = \frac{\hat{p}^2}{2m} + \frac{1}{2} m \Omega^2 \hat{x}^2, \quad (5)$$

$$\hat{H}_{\text{res}} = \sum_{l,r} \varepsilon_l \hat{c}_l^\dagger \hat{c}_l + \varepsilon_r \hat{c}_r^\dagger \hat{c}_r, \quad (6)$$

where \hat{H}_{osc} describes the oscillator with \hat{x} and \hat{p} being the position and momentum operator of the oscillator with mass m and frequency Ω , respectively. \hat{H}_{res} contains the fermionic reservoirs of the left and right contacts. The oscillator couples to the tunnel junction via the tunneling Hamiltonian

$$\hat{H}_{\text{tun}} = \sum_{l,r} \beta \hat{c}_l^\dagger \hat{c}_r + \text{H.c.} \quad (7)$$

Here \hat{c}_i (\hat{c}_i^\dagger) annihilates (creates) an electron in reservoir $i = l, r$. Motivated by the experimental setup in Ref. 20, we take the oscillator to act as one of the fermionic reservoirs. Therefore the tunneling gap depends on the position of the oscillator, modifying the tunneling amplitude of the APC. For small oscillator displacements x , we assume linear coupling of the oscillator to the tunnel junction with a tunnel amplitude β_1 . Hence we obtain $\beta = [\beta_0 + \beta_1 \hat{x}]$, with β_0 being the bare tunneling amplitude. Here, we allow for complex tunnel amplitudes β_0 and β_1 as previously discussed in Refs. 17 and 21. With η we denote the relative phase between the tunnel amplitudes, i.e., we write $\beta_0 = t_0$ and $\beta_1 = t_1 e^{i\eta}$ where $t_0, t_1 \in \Re$. A possible experimental realization of the finite and tunable phase η is discussed in Ref. 17. As a consequence, this phase η gives rise to the possibility to detect the oscillator's momentum expectation value $\langle \hat{p}^2 \rangle$, present in the current noise.

IV. GREEN'S FUNCTIONS OF THE FERMIONIC RESERVOIR AND OF THE OSCILLATOR USING THE KELDYSH TECHNIQUE

The true nonequilibrium, non-Markovian quantum behavior of the coupled system is the subject of our interest. Therefore we make use of the Keldysh formalism^{22,23} for our calculation. The quantities being accessible in the experiment are, for instance, the tunnel current and the current-current correlator, the noise of the tunnel junction. These will also be the main objects of interest in this paper. We employ a perturbation theory in the tunnel Hamiltonian \hat{H}_{tun} and calculate the noise up to fourth order in the tunneling.

The current operator is given by $\hat{I} = -e\hat{N}_l$, where $\hat{N}_l = \hat{c}_l^\dagger \hat{c}_l$ counts electrons in the left reservoir. We then write the current operator as

$$\hat{I} = e[\hat{j}_0 + \hat{x}\hat{j}_1] \quad (8)$$

and similarly

$$\hat{H}_{\text{tun}} = \hat{h}_0 + \hat{x}\hat{h}_1, \quad (9)$$

with $\hat{j}_i = i[\hat{T}_i - \hat{T}_i^\dagger]$ and $\hat{h}_i = \hat{T}_i + \hat{T}_i^\dagger$. The operator \hat{T}_i is given by $\hat{T}_i = \sum_{l,r} \beta_i \hat{c}_i^\dagger \hat{c}_r$ with $i \in \{0,1\}$.

A. Reservoirs Green's functions

The fermionic Green's functions of the left and right reservoirs (free-electron gas) $G_{l,r}$, are given on the Keldysh contour C by $G_{l,r}(t,t') = -i\langle T_c \hat{c}_{l,r}(t) \hat{c}_{l,r}^\dagger(t') \rangle$. T_c denotes the time ordering operator on the Keldysh contour, placing times lying further along the contour to the left. Figure 2 shows the Keldysh contour C . The contour consists of a lower branch, C_- on which time evolves in the forward direction and of an upper branch C_+ , where time evolves in the backward direction. Switching from times lying on the contour to real times is done by analytic continuation. The Keldysh Green's functions $G_{l,r}(t,t')$ can then be represented by a matrix. A Fourier transformation leads to the following Green's functions:

$$\begin{aligned} G_{l,r}(\omega) &= \begin{pmatrix} G_{l,r}^{--}(\omega) & G_{l,r}^{-+}(\omega) \\ G_{l,r}^{+-}(\omega) & G_{l,r}^{++}(\omega) \end{pmatrix} \\ &= 2\pi i \rho_0 \begin{pmatrix} n_{l,r}(\omega) - 1/2 & n_{l,r}(\omega) \\ n_{l,r}(\omega) - 1 & n_{l,r}(\omega) - 1/2 \end{pmatrix}. \end{aligned} \quad (10)$$

Here we made use of time translation invariance and assumed a constant density of states in the left and right reservoir $\rho_l = \rho_r = \rho_0$. We make the reasonable assumption that the fermionic bath relaxes much faster than the system into a steady state, justifying that the fermionic bath correlation functions do not depend on absolute times but only on the time difference. The applied finite bias $\mu_r - \mu_l = eV$ is included in the Fermi distribution functions $n_l =$

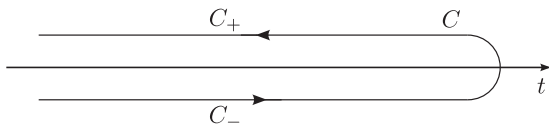


FIG. 2. Keldysh contour C with the lower branch C_- and the upper branch C_+ .

$n(\omega - eV/2) = [\exp(\beta(\omega - eV/2) + 1)]^{-1}$ and $n_r = n(\omega + eV/2) = [\exp(\beta(\omega + eV/2) + 1)]^{-1}$. The inverse temperature of electrons in the reservoirs is $\beta = 1/k_B T$ and we use units where $\hbar = 1$.

B. Oscillator

Since the oscillator modulates the tunneling of electrons and therefore has impact on the measured average current and current-current correlator, it is important to understand the significance of the oscillator's state. We distinguish between an oscillator in a stationary state and one in a nonstationary state. We justify this differentiation by arguing that for short times after the measurement, the oscillator will certainly be nonstationary. The dominating time scale here is the one given by the oscillator itself, $1/\Omega$, which has to be compared to times scales on which the damping of the oscillator due to the tunnel junction and the external heat bath happens. In the nonstationary case, we cannot make use of time translation invariance in the oscillator's correlation function $D(t,t')$. For longer times however, the assumption of stationarity is justified since the oscillator can equilibrate with the environment and reach a steady state. The oscillator's correlation function now only depends on the time difference $t - t'$.

We work in the following with the oscillator operators given in the Heisenberg picture as $\hat{x}(t) = \hat{x} \cos(\Omega t) + \hat{p}/(m\Omega) \sin(\Omega t)$ and $\hat{p}(t) = \hat{p} \cos(\Omega t) - \hat{x}(m\Omega) \sin(\Omega t)$. We also define the aforementioned oscillator correlation function $D(t,t')$ in Keldysh space as

$$D(t,t') = -i\langle T_c \hat{x}(t) \hat{x}(t') \rangle. \quad (11)$$

When we later investigate the second-order noise we consider both the stationary situation and the nonstationary situation. The following relation then is a very useful one:

$$\hat{x}(t + t') = \hat{x}(t') \cos(\Omega t) + \frac{\hat{p}(t')}{m\Omega} \sin(\Omega t). \quad (12)$$

For calculations up to second order, we look at the influence of stationary and nonstationary oscillator states on the current noise; in fourth order we restrict ourselves to the stationary case. Hence we are interested in a clear definition of the oscillator's correlation functions and spectral functions in the stationary case, which will be addressed now.

1. Oscillator correlation functions in the stationary case

Considering the stationary case, we give useful expressions for the oscillator's correlation functions, which later allow us to identify the oscillator's power spectrum in x denoted by $S_x(\omega)$ and in p denoted by $S_p(\omega)$. From Eq. (11) the correlation function where $t \in C_+$ and $t' \in C_-$ is given by

$$\begin{aligned} iD^{+-}(t,t') &= \langle \hat{x}(t) \hat{x}(t') \rangle \\ &= \frac{1}{2} \left\langle \bar{x}_+^2 \cos[\Omega(t - t')] + \frac{[\hat{p}, \hat{x}]}{m\Omega} \sin[\Omega(t - t')] \right. \\ &\quad \left. + \bar{x}_-^2 \cos[\Omega(t + t')] + \frac{[\hat{p}, \hat{x}]}{m\Omega} \sin[\Omega(t + t')] \right\rangle. \end{aligned} \quad (13)$$

and similar for $t \in C_-$ and $t' \in C_+$

$$\begin{aligned} iD^{-+}(t, t') &= \langle \hat{x}(t') \hat{x}(t) \rangle \\ &= \frac{1}{2} \left\langle \bar{x}_+^2 \cos[\Omega(t - t')] - \frac{[\hat{p}, \hat{x}]}{m\Omega} \sin[\Omega(t - t')] \right. \\ &\quad \left. + \bar{x}_-^2 \cos[\Omega(t + t')] + \frac{[\hat{p}, \hat{x}]}{m\Omega} \sin[\Omega(t + t')] \right\rangle, \end{aligned} \quad (14)$$

where we defined

$$\bar{x}_\pm^2 = \hat{x}^2 \pm \frac{\hat{p}^2}{m^2\Omega^2}, \quad (15)$$

and $[\cdot, \cdot]$ denotes the commutator and $\{\cdot, \cdot\}$ the anticommutator. Since, here we deal with the stationary case, the expectation values $\langle \bar{x}_\pm^2 \rangle$ and $\langle [\hat{p}, \hat{x}] \rangle$ appearing as prefactors of functions depending on $t + t'$ equal to zero, which one can easily check by using any stationary state, e.g., number states. As one would expect, the correlation function now is a function of the time difference $t - t'$ only. The Fourier transform of the correlation functions then yields

$$iD^{+-}(\omega) = \frac{1}{2} \left\langle \bar{x}_+^2 \mathcal{R}_\gamma^+(\omega, \Omega) + \frac{i[\hat{p}, \hat{x}]}{m\Omega} \mathcal{R}_\gamma^-(\omega, \Omega) \right\rangle, \quad (16)$$

$$iD^{-+}(\omega) = \frac{1}{2} \left\langle \bar{x}_+^2 \mathcal{R}_\gamma^+(\omega, \Omega) - \frac{i[\hat{p}, \hat{x}]}{m\Omega} \mathcal{R}_\gamma^-(\omega, \Omega) \right\rangle. \quad (17)$$

Additionally, we introduce the two momentum correlation functions $iP^{+-}(t, t') = \langle \hat{p}(t) \hat{p}(t') \rangle$ and $iP^{-+}(t, t') = \langle \hat{p}(t') \hat{p}(t) \rangle$. The same arguments as for $iD^{\pm\mp}(t, t')$ lead here to the following Fourier transforms:

$$iP^{+-}(\omega) = \frac{1}{2} \langle \bar{p}_+^2 \mathcal{R}_\gamma^+(\omega, \Omega) + m\Omega i [\hat{p}, \hat{x}] \mathcal{R}_\gamma^-(\omega, \Omega) \rangle, \quad (18)$$

$$iP^{-+}(\omega) = \frac{1}{2} \langle \bar{p}_+^2 \mathcal{R}_\gamma^+(\omega, \Omega) - m\Omega i [\hat{p}, \hat{x}] \mathcal{R}_\gamma^-(\omega, \Omega) \rangle, \quad (19)$$

where, similar to above,

$$\bar{p}_\pm^2 = m^2\Omega^2 \hat{x}^2 \pm \hat{p}^2. \quad (20)$$

We introduce the functions $\mathcal{R}_\gamma^\pm(\omega, \Omega)$ as

$$\mathcal{R}_{\gamma \rightarrow 0}^+(\omega, \Omega) = \pi[\delta(\omega + \Omega) + \delta(\omega - \Omega)], \quad (21)$$

$$\mathcal{R}_{\gamma \rightarrow 0}^-(\omega, \Omega) = \pi[\delta(\omega - \Omega) - \delta(\omega + \Omega)]. \quad (22)$$

The coupling of the oscillator to two environments, namely an external heat bath and the tunnel junction, being at the temperatures T_{env} and $k_B T_{\text{junc}} = eV/2$,²⁴ respectively, introduces a damping of the oscillator with damping coefficients γ_0 and γ_+ , respectively. The oscillator dynamics due to the coupling to the tunnel junction can be calculated by solving a Dyson equation for the oscillator correlation function $D(t, t')$ where the self-energy is taken to lowest nonvanishing order in the tunnel Hamiltonian, i.e., $\Sigma(t, t') = -i \langle T_c \hat{h}_1(t) \hat{h}_1(t') \rangle$. Using the Keldysh technique, as was done in Refs. 18 and 25, the oscillator dynamics and the damping coefficient $\gamma_+ = \pi \rho_0^2 t_1^2 / m$ can be calculated. The coupling to the external heat bath can be added phenomenologically, or particularly as an interaction with a bath of harmonic oscillators. The total damping then follows as $\gamma_{\text{tot}} = \gamma_0 + \gamma_+$. We can assign

an effective temperature T_{eff} to the oscillator with $\gamma_{\text{tot}} T_{\text{eff}} = \gamma_+ T_{\text{junc}} + \gamma_0 T_{\text{env}}$. This leads to the general case for \mathcal{R}_γ^\pm by replacing the δ functions in Eqs. (21) and (22) by a Lorentzian, where we include both sources of damping and an oscillator frequency $\Omega \rightarrow \sqrt{\Omega^2 - \gamma^2}$. For this damped case we can write for $\mathcal{R}_\gamma^+(\omega, \Omega)$ and $\mathcal{R}_\gamma^-(\omega, \Omega)$

$$\mathcal{R}_\gamma^+(\omega, \Omega) = \frac{2\gamma_{\text{tot}}(\omega^2 + \Omega^2)}{4\gamma_{\text{tot}}^2\omega^2 + (\omega^2 - \Omega^2)^2}, \quad (23)$$

$$\mathcal{R}_\gamma^-(\omega, \Omega) = \frac{4\gamma_{\text{tot}}\omega\sqrt{\Omega^2 - \gamma_{\text{tot}}^2}}{4\gamma_{\text{tot}}^2\omega^2 + (\omega^2 - \Omega^2)^2}. \quad (24)$$

We want to stress that we have not made any assumption on the initial time as, e.g., $t' = 0$. This concludes our discussion on the oscillator correlation functions. We now turn to the spectral functions $S_x(\omega)$ and $S_p(\omega)$.

2. The oscillator's spectra in the stationary case

The symmetrized power spectrum, in general defined as $\frac{1}{2} \int dt e^{i\omega t} \langle \{\hat{Y}(t), \hat{Y}(t')\} \rangle$ of the oscillator quantities $\hat{Y} = \hat{x}, \hat{p}$ is an observable that can be measured by, e.g., current noise measurements (as discussed below). Both $S_x(\omega)$ and $S_p(\omega)$ can be measured through the current noise $S_{\text{sym}}(\omega)$. The expressions for these power spectra are given by

$$S_x(\omega) = \frac{1}{2} \int dt e^{i\omega t} \langle \{\hat{x}(t), \hat{x}(t')\} \rangle = \frac{1}{2} \langle \bar{x}^2 \rangle \mathcal{R}_\gamma^+(\omega, \Omega), \quad (25)$$

and

$$S_p(\omega) = \frac{1}{2} \int dt e^{i\omega t} \langle \{\hat{p}(t), \hat{p}(t')\} \rangle = \frac{1}{2} \langle \bar{p}^2 \rangle \mathcal{R}_\gamma^+(\omega, \Omega). \quad (26)$$

The momentum and position spectrum are related via the relation

$$S_p(\omega) = m^2\Omega^2 S_x(\omega). \quad (27)$$

We can also write down the spectra using the Keldysh Green's function $D^K(\omega) = D^{+-}(\omega) + D^{-+}(\omega)$, which yields

$$S_x(\omega) = \frac{i}{2} D^K(\omega), \quad (28)$$

$$S_p(\omega) = \frac{i}{2} m^2\Omega^2 D^K(\omega). \quad (29)$$

To further simplify the notation, we introduce

$$Q(\omega) = \frac{i}{2} [\Upsilon^{+-}(\omega) - \Upsilon^{-+}(\omega)] = \frac{1}{2m\Omega} \mathcal{R}_\gamma^-(\omega, \Omega), \quad (30)$$

where $\Upsilon = D, P$ which is used later in the fourth-order noise calculation.

V. CURRENT NOISE CALCULATIONS

In this section, we cover a variety of aspects when dealing with the current noise. For all different aspects we find expressions for the noise which are valid for an arbitrary η and therefore include the x detector as well as the p detector.

The first part is dedicated to the noise in second-order perturbation theory, where we furthermore make the distinction between a stationary harmonic oscillator and a nonstationary one. Besides the Markovian regime ($eV \gg \hbar\Omega$), the Keldysh formalism also allows us to investigate the non-Markovian regime ($eV \ll \hbar\Omega$). The main results in this section are that

the current noise for a nonstationary oscillator can in principle be complex. In this case, a detectable complex noise would allow for a nearly complete determination of the oscillator's covariance matrix $\sigma_{ij} = \text{tr}(\hat{\rho} \{\hat{Y}_i, \hat{Y}_j\}/2)$, where $\hat{Y} = (\hat{x}, \hat{p})^T$. The covariance matrix allows for a complete description of the oscillator's quantum state.

For the stationary oscillator we recover a noise that is real and in accordance with the Wiener-Khinchin theorem. This noise is the well-known noise of a bare biased tunnel junction which shows kinks at $|\omega| = |V|$,^{26,27} modified by the oscillator leading to kinks at $|\omega| = |V \pm \Omega|$.

In the last part of this section, we deal with the noise up to fourth order in the tunneling amplitudes. Then we restrict ourselves on the stationary case. On the one hand, the fourth-order contributions modify the kinks, on the other hand, they give rise to resonances stemming from the oscillator correlation functions.^{14,17,18}

Importantly, we study the problem over the whole parameter range. Thus, we go, e.g., beyond Ref. 15 where a Markov approximation was employed and lead to the constraint $\Omega \ll \max(k_B T, eV)$ for the high-frequency current noise. Before we introduce the perturbation theory leading to the noise expression, we want to clarify the term second- and fourth-order perturbation theory. When we talk about these two cases we want to indicate that we expanded the quantities that we calculated to second and fourth order in the tunneling amplitudes. Our results, especially in Sec. VC, are of higher order than the actual expansion since we used the oscillator Green's function Eq. (11), which is obtained by solving the Dyson equation with the proper self-energy as discussed in Sec. IV B 1.

A. Overview

In general, the expression for the current-current correlator in the Keldysh formalism is given by (expectation values are taken with respect to the unperturbed Hamiltonian, i.e., the Hamiltonian without \hat{H}_{tun})

$$S(\tau_3, \tau_4) = \langle T_c e^{-i \int_c d\bar{\tau} \hat{H}_{\text{tun}}(\bar{\tau})} \hat{I}(\tau_3) \hat{I}(\tau_4) \rangle_0 - \langle \hat{I}(\tau_3) \rangle_0 \langle \hat{I}(\tau_4) \rangle_0, \quad (31)$$

since we consider only the second- and fourth-order current noise we write

$$S(\tau_3, \tau_4) = S^{(2)}(\tau_3, \tau_4) + S^{(4)}(\tau_3, \tau_4), \quad (32)$$

where

$$S^{(2)}(\tau_3, \tau_4) = \langle T_c \hat{I}(\tau_3) \hat{I}(\tau_4) \rangle_0, \quad (33)$$

and

$$\begin{aligned} S^{(4)}(\tau_3, \tau_4) &= -\frac{1}{2} \int_c d\tau_1 d\tau_2 \langle T_c \hat{H}_{\text{tun}}(\tau_1) \hat{H}_{\text{tun}}(\tau_2) \hat{I}(\tau_3) \hat{I}(\tau_4) \rangle_0 \\ &+ \int_c d\tau_1 d\tau_2 \langle T_c \hat{H}_{\text{tun}}(\tau_1) \hat{I}(\tau_3) \rangle_0 \langle T_c \hat{H}_{\text{tun}}(\tau_2) \hat{I}(\tau_4) \rangle_0. \end{aligned} \quad (34)$$

The general expression for the average current is given by

$$\langle I(t) \rangle = \langle T_c e^{-i \int_c d\tau \hat{H}_{\text{tun}}(\tau)} \hat{I}(t) \rangle_0. \quad (35)$$

To second order in the tunneling amplitudes, the average current can be calculated by

$$\langle I(t) \rangle = -i \int_c d\tau (T_c \hat{H}_{\text{tun}}(\tau) \hat{I}(t))_0, \quad (36)$$

and we obtain

$$\begin{aligned} \langle I(t) \rangle &= 2\pi \rho_0^2 e \left\{ t_0^2 eV + 2 \cos(\eta) t_0 t_1 eV \langle \hat{x}(t) \rangle + \sin(\eta) t_0 t_1 \right. \\ &\quad \times \left. \frac{\langle \hat{p}(t) \rangle}{m} + t_1^2 eV \langle \hat{x}(t) \hat{x}(t) \rangle - \frac{t_1^2}{2m\Omega} \sigma^-(\Omega, V) \right\}, \end{aligned} \quad (37)$$

where $\sigma^-(\Omega, V)$ is given in Eq. (42) below. Our result for the average current is in accordance with Ref. 17. The current noise we calculate is always the frequency-dependent (and in the nonstationary case also time-dependent) symmetrized current noise, defined as

$$S_{\text{sym}}(\omega, t') = \frac{1}{2} \int dt e^{i\omega t} [S^{-+}(t, t') + S^{+-}(t, t')], \quad (38)$$

where for $S^{-+}(t, t')$, $t \in C_-$ and $t' \in C_+$ and similarly for $S^{+-}(t, t')$, here C_- and C_+ are the lower and upper branch of the Keldysh contour C , respectively; see Fig. 2. The debate whether the symmetrized or unsymmetrized current noise of the detector is accessible in an experiment has been discussed in Refs. 28 and 29. We focus on the symmetrized version of the current noise, since leading experiments as in Refs. 20 and 27 showed that the symmetrized current noise is measurable and since the focus of this paper lies in the characterization of the nanomechanical resonator.

B. Current noise to second order in the tunneling amplitudes

We now turn to the calculation of the current noise to second order. With the current operator \hat{I} already being first order in the tunneling amplitudes, the current noise in the Born approximation is given by the following expression:

$$S^{(2)ij}(t, t') = \langle T_c \hat{I}(t + t')_i \hat{I}(t')_j \rangle, \quad (39)$$

where we used a slightly different definition of the current noise. This definition will be useful when examining the nonstationary case. Due to this definition the time dependence on t' in the symmetrized current noise is only present in the oscillator's quantum-mechanical expectation values.

The general expression for the current noise in Keldysh space reads

$$\begin{aligned} S^{(2)ij}(t, t') &= e^2 [\mathcal{G}_{00}(t + t', t') + \langle \hat{x}(t') \rangle \mathcal{G}_{01}(t + t', t') \\ &\quad + \langle \hat{x}(t + t') \rangle \mathcal{G}_{10}(t + t', t') \\ &\quad + i D(t + t', t') \mathcal{G}_{11}(t + t', t')], \end{aligned} \quad (40)$$

where $\mathcal{G}_{ij}(t, t')$ is given in Appendix A.

1. General expression for the current noise

In this section, we only make use of time translation invariance in the $\mathcal{G}_{ij}(t, t')$ functions; the oscillator is taken as nonstationary. Details of the calculation can be found in Appendix B. The final result we obtain for the symmetrized

current noise to second order in the tunneling amplitudes reads

$$\begin{aligned}
S_{\text{sym}}^{(2)}(\omega, t') = & 2\pi\rho_0^2 e^2 \left\{ t_0^2 \sigma^+(\omega, V) + \langle \hat{x}(t') \rangle t_0 t_1 \cos(\eta) \left[\sigma^+(\omega, V) + \frac{1}{2} [\sigma^+(\omega + \Omega, V) + \sigma^+(\omega - \Omega, V)] \right] \right. \\
& - \langle \hat{x}(t') \rangle t_0 t_1 i \sin(\eta) \left[\sigma^-(\omega, V) - \frac{1}{2} [\sigma^-(\omega + \Omega, V) + \sigma^-(\omega - \Omega, V)] \right] - \langle \hat{p}(t') \rangle \frac{t_0 t_1}{2m\Omega} [\sin(\eta) [\sigma^-(\omega + \Omega, V) \\
& - \sigma^-(\omega - \Omega, V)] - i \cos(\eta) [\sigma^+(\omega + \Omega, V) - \sigma^+(\omega - \Omega, V)] + \langle \hat{x}(t') \hat{x}(t') \rangle \frac{t_1^2}{2} [\sigma^+(\omega + \Omega, V) + \sigma^+(\omega - \Omega, V)] \\
& \left. - \frac{t_1^2}{2m} - \langle \{\hat{x}(t'), \hat{p}(t')\} \rangle \frac{i t_1^2}{4m\Omega} [\sigma^+(\omega + \Omega, V) - \sigma^+(\omega - \Omega, V)] \right\}, \quad (41)
\end{aligned}$$

where we separated the real and imaginary part using the relative phase η between the tunneling amplitudes and in addition introduced

$$\begin{aligned}
\sigma^\pm(\xi, V) = & \frac{eV + \xi}{2} \coth\left(\beta \frac{eV + \xi}{2}\right) \\
& \pm \frac{eV - \xi}{2} \coth\left(\beta \frac{eV - \xi}{2}\right). \quad (42)
\end{aligned}$$

We want to note the important aspect of the current noise that it possibly can have a complex valued character which we discuss later. The gained expression is quite lengthy but provides us with the full quantum-mechanical nonequilibrium characteristics of the current noise in the Markovian as well as in the non-Markovian regime. We made no assumptions on the state of the oscillator, which now gives us the possibility to identify momentum properties of the nanomechanical resonator using the current noise spectrum $S_{\text{sym}}^{(2)}(\omega, t')$. In the next section, we discuss this new possibility of a p detector, which involves measuring a complex valued current noise.

2. Complex current noise and the p detector in the nonstationary case

The expression in Eq. (41) allows for a comparison with results obtained in Ref. 17 where it was possible with a phase of $\eta = \pi/2$ to determine the momentum of the oscillator. In Ref. 17 an Aharonov-Bohm setup allows the tuning of the relative phase η . The full current noise spectrum there is proportional to the position spectrum $S_x(\omega)$ which is peaked at $\omega = \pm\Omega$ in the case of $\eta = 0$ and in the case of $\eta = \pi/2$ is proportional to the momentum spectrum $S_p(\omega)$ showing peaks at $\omega = \pm\Omega$. This peaked structure of the current noise spectrum is a fourth-order effect, as we will see and discuss later when dealing with the fourth-order corrections to the current noise.

As one can see from Eq. (41), already the second-order current noise allows us to determine the expectation value of the oscillator's momentum and in addition to that of the anticommutator $\{\hat{x}, \hat{p}\}$, even if the phase $\eta = 0$, i.e., the Aharonov-Bohm setup becomes obsolete in our case. The signature of the oscillator's momentum \hat{p} in our case is, however, different than the one in Ref. 17. Instead of the peaked structure, we find a kinklike structure, which stems from the fact that we deal with second-order perturbation theory.

In order to understand how one can use this to identify the momentum, we have to understand the meaning of a

complex current noise. As stated in Ref. 30, a complex valued current noise is in principle a measurable quantity. To have a relevant measurable quantity we would have to average the time-dependent current noise $S_{\text{sym}}^{(2)}(\omega, t')$ over the measurement time ΔT . We could do this in the following way:

$$\bar{S}_{\text{sym}}^{(2)}(\omega) = \frac{1}{\Delta T} \int_{-\Delta T/2}^{\Delta T/2} dt' S_{\text{sym}}^{(2)}(\omega, t'). \quad (43)$$

Since the time dependence of the current noise is only visible in the expectation values of the oscillator's variables, it is important for the actual measurement to consider the time scales which are involved. If the measurement time ΔT is less than the time scale of the oscillator ($1/\Omega$), the measured time averaged current noise $\bar{S}_{\text{sym}}^{(2)}(\omega)$ will be time dependent. If, however, the oscillator undergoes multiple oscillation cycles during the measurement time, the current noise will be time independent. In this case we could as well take the oscillator to be in a stationary state. For a damped oscillator the time scales on which the damping happens have to be taken into account, as mentioned already in Sec. IV B.

Let us briefly discuss the involved time scales for the experiment in Ref. 20. The oscillator with a quality factor of $Q_0 \approx 5000$ at frequency $\Omega \approx 60$ MHz has a typical relaxation time scale of $\tau_{\text{osc}} \approx 100$ μs . For low temperatures the quasiparticle relaxation rate of the fermionic reservoirs can be estimated by usual Fermi-liquid theory ($1/\tau_{\text{res}} \sim T^2$),³¹ which leads for 250 mK used in the experiment to a relaxation time scale τ_{res} of order μs . Hence $\tau_{\text{res}} \ll \tau_{\text{osc}}$ in Ref. 20. Furthermore, the detector in Ref. 20 has a high enough resolution of measuring displacements on time scales less than 10 ns.

We conclude with remarks on the interesting nonstationary case, where we can also take $\eta = 0$ without losing the information on $\langle \hat{p}(t') \rangle$, and in addition obtain information on $\langle \{\hat{x}(t'), \hat{p}(t')\} \rangle$. We intend to give an idea of how to access the information on $\langle \hat{p}(t') \rangle$ and $\langle \{\hat{x}(t'), \hat{p}(t')\} \rangle$ available through the complex current noise.

The expectation value of $\langle \hat{p}(t') \rangle$, with respect to number states or a linear combination of them, will always vanish when averaging over time according to Eq. (43). However, this is different for coherent states $|\alpha\rangle = \exp(-|\alpha|^2/2) \sum_{n=0}^{\infty} \alpha^n/n! |n\rangle$, where we can write $\alpha = |\alpha| \exp(i\delta)$ with $|\alpha|$ being the amplitude and δ the phase of the coherent state, respectively. The

time-averaged expectation values $\langle \hat{p}(t') \rangle$ and $\langle \{\hat{x}(t'), \hat{p}(t')\} \rangle$ with respect to $|\alpha\rangle$ yield

$$\langle \hat{p}(t') \rangle_{\text{av}} = \sqrt{2m\Omega} \frac{2|\alpha|}{\Omega\Delta T} \sin(\delta) \sin(\Omega\Delta T/2), \quad (44)$$

and

$$\langle \{\hat{x}(t'), \hat{p}(t')\} \rangle_{\text{av}} = \frac{2|\alpha|^2}{\Omega\Delta T} \sin(2\delta) \sin(\Omega\Delta T), \quad (45)$$

where $\langle \cdot \rangle_{\text{av}}$ contains two averages, the quantum mechanical average denoted by $\langle \cdot \rangle$ and the time average according to Eq. (43) denoted by the subscript av.

For short measurement times $\Delta T < 1/\Omega$ we can write

$$\lim_{\Delta T \rightarrow 0} \langle \hat{p}(t') \rangle_{\text{av}} = \sqrt{2m\Omega} |\alpha| \sin(\delta), \quad (46)$$

$$\lim_{\Delta T \rightarrow 0} \langle \{\hat{x}(t'), \hat{p}(t')\} \rangle_{\text{av}} = 2|\alpha|^2 \sin(2\delta). \quad (47)$$

We separate the current noise $\bar{S}_{\text{sym}}^{(2)}(\omega) = \bar{S}_{\text{sym,R}}^{(2)}(\omega) + \bar{S}_{\text{sym,I}}^{(2)}(\omega)$ into real and imaginary parts where we observe that the imaginary part $\bar{S}_{\text{sym,I}}^{(2)}(\omega)$ only contains information on the oscillator's momentum $\langle \hat{p}(t') \rangle$ and the anticommutator $\langle \{\hat{x}(t'), \hat{p}(t')\} \rangle$,

$$\begin{aligned} \bar{S}_{\text{sym,I}}^{(2)}(\omega) = & 2\pi\rho_0^2 e^2 \left\{ \frac{1}{\sqrt{2m\Omega}} t_0 t_1 |\alpha| \sin(\delta) [\sigma^+(\omega + \Omega, V) \right. \\ & - \sigma^+(\omega - \Omega, V)] - \frac{t_1^2 |\alpha|^2}{2m\Omega} \sin(2\delta) \\ & \left. \times [\sigma^+(\omega + \Omega, V) - \sigma^+(\omega - \Omega, V)] \right\}. \quad (48) \end{aligned}$$

The phase δ of the coherent state now allows for a determination of the oscillator's momentum. For $\delta = \pi/2$, the signature in the imaginary part of the time-averaged noise $\bar{S}_{\text{sym,I}}^{(2)}(\omega)$ stems only from the oscillator's momentum. The signal in the non-Markovian regime is more pronounced than in the Markovian regime; see Eq. (48).

3. Current noise in the stationary case

Contrary to the nonstationary case we now also assume time translation invariance in the oscillator correlation function, i.e., $D(t, t') = D(t - t')$. One can see that the calculation in the stationary case goes along the same lines as in the nonstationary case. The only difference will be that oscillator expectation values are now taken at time $t' = 0$, i.e., we encounter, for instance, $\langle \hat{x}(0) \rangle$ instead of $\langle \hat{x}(t') \rangle$.

When interpreting the result for the stationary case we have to keep the constraints on oscillator expectation values in mind. These constraints mentioned in Sec. IV B 1 lead to vanishing expectation values of the anticommutator $\langle \{\hat{x}, \hat{p}\} \rangle$ and vanishing expectation values for $\langle \hat{x} \rangle$ and $\langle \hat{p} \rangle$. The current noise to second order is then equivalent to the ones previously obtained in Refs. 18 and 21, cf. Eq. (C.4) in the supplemental material of Ref. 21 with $\gamma_2 = \langle x \rangle = \langle p \rangle = 0$.

C. Current noise to fourth order in the tunneling amplitudes

We now turn to the investigation of the fourth-order current noise. Since the fourth-order perturbation theory involves a large amount of terms we use a diagrammatic approach. In the case of the fourth-order current noise we restrict ourselves to the stationary case for simplicity. An overview

of all contributing terms in the nonstationary case is given in Appendix C. In what follows we give a short explanation of the diagrammatics. From Eq. (34) it becomes obvious that $S^{(4)}$ contains fermionic expectation values which have the form

$$\begin{aligned} \mathcal{M}_{i_1, i_2, i_3, i_4}(\tau_1, \tau_2, \tau_3, \tau_4) &= \langle T_c \hat{h}_{i_1}(\tau_1) \hat{h}_{i_2}(\tau_2) \hat{j}_{i_3}(\tau_3) \hat{j}_{i_4}(\tau_4) \rangle \\ &= \langle T_c \mathcal{T}_{i_1}^\dagger(\tau_1) \mathcal{T}_{i_2}(\tau_2) \mathcal{T}_{i_3}(\tau_3) \mathcal{T}_{i_4}^\dagger(\tau_4) \\ &\quad + (3 \leftrightarrow 4) - (2 \leftrightarrow 4) + \text{H.c.} \rangle. \quad (49) \end{aligned}$$

The index i_j determines whether we are dealing with β_0 or β_1 , $i_j \in \{0, 1\}$. It is only necessary to evaluate the first expectation value in Eq. (49) using Wick's theorem; the other ones follow as indicated by $(3 \leftrightarrow 4)$, $(2 \leftrightarrow 4)$ and Hermitian conjugation. This first term leads to

$$\begin{aligned} & \langle T_c \mathcal{T}_{i_1}^\dagger(\tau_1) \mathcal{T}_{i_2}(\tau_2) \mathcal{T}_{i_3}(\tau_3) \mathcal{T}_{i_4}^\dagger(\tau_4) \rangle \\ &= \beta_{i_1}^* \beta_{i_2} \beta_{i_3} \beta_{i_4}^* [G_l(\tau_1, \tau_2) G_l(\tau_4, \tau_3) - G_l(\tau_1, \tau_3) G_l(\tau_4, \tau_2)] \\ &\quad \times [G_r(\tau_2, \tau_1) G_r(\tau_3, \tau_4) - G_r(\tau_3, \tau_1) G_r(\tau_2, \tau_4)]. \quad (50) \end{aligned}$$

Similar to Ref. 18, we use a diagrammatic representation for the expression in Eq. (49). As an example, we show the diagrams emerging from the expression in Eq. (50) in Fig. 3 and explain the components of the diagrams. Fermionic Green's functions of the reservoirs are represented by solid lines and vertices are depicted by a dot, labeled with a time variable and a Keldysh index indicating on which branch of the Keldysh contour the time lies. An integration over internal times τ_1 and τ_2 is implicit. In addition we also have to sum over the two internal Keldysh indices k and l . We recognize that we have to deal with two types of diagrams: diagrams which consist of one closed fermion loop (diagrams in the lower panel of Fig. 3) and diagrams consisting of two closed fermion loops or bubbles (diagrams in the upper panel of Fig. 3). These two different types of diagrams give very different contributions to the current noise, which we will discuss below. We include the oscillator correlation function $D(t, t')$ in diagrams by a wiggly line connecting two vertices. In Fig. 4, we give an example of diagrams in frequency space containing one oscillator correlation function. Here, integration over the two internal frequencies ω_1 and ω_2 as well as summation over the internal Keldysh indices k and l is implied. In frequency space the difference between the closed-loop diagrams, (b) in Fig. 4, and the bubble diagrams, (a) in Fig. 4, becomes clear: for the closed-loop diagrams, the oscillator line always appears under integration of an internal frequency, whereas for the bubble diagrams, there is no integration over the oscillator line. This is the reason for the different kinds of contribution to the current noise of closed-loop and bubble diagrams. As we will show below, bubble diagrams lead to peaks in the current noise, whereas closed-loop diagrams lead to the aforementioned kinks in the current noise. We reduce the number of diagrams by only keeping contributions $\sim t_0^2 t_1^2$ and $\sim t_1^4$, which are the only finite contributions in the stationary case. Details are given in Appendix C. This allows us to write the current noise $S^{(4)}(\tau_3, \tau_4)$ for the further analysis as

$$\begin{aligned} S^{(4)}(\tau_3, \tau_4) &= \hat{S}_D^{(4)}(\tau_3, \tau_4) + \check{S}_D^{(4)}(\tau_3, \tau_4) \\ &\quad + \hat{S}_{DD}^{(4)}(\tau_3, \tau_4) + \check{S}_{DD}^{(4)}(\tau_3, \tau_4), \quad (51) \end{aligned}$$

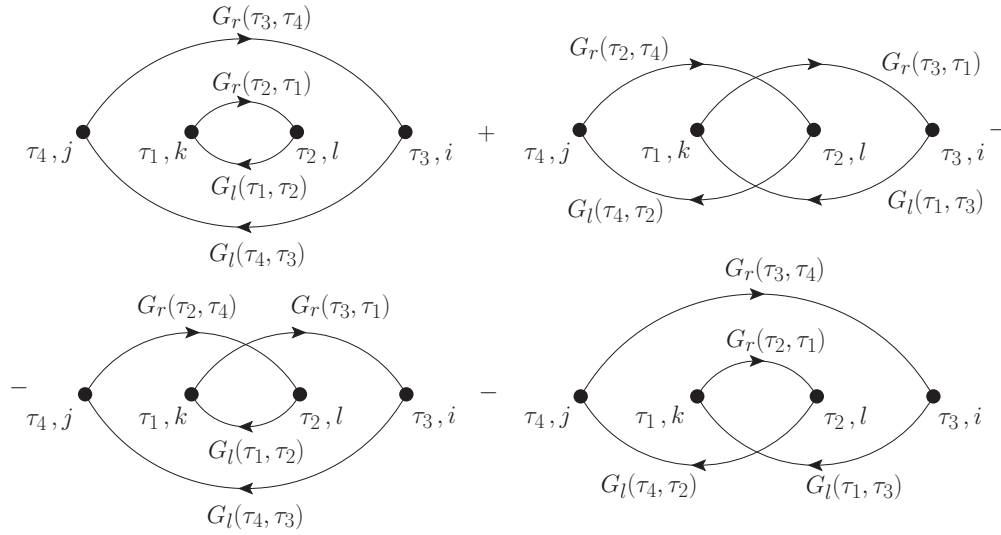


FIG. 3. Diagrammatic representation for Eq. (50) where we omitted the factor $\beta_{i_1}^* \beta_{i_2} \beta_{i_3} \beta_{i_4}^*$; note that Eq. (50) only contains fermionic Green's functions.

where \hat{S} includes the bubble diagrams, \check{S} includes closed-loop diagrams and D indicates the number of oscillator lines in the diagrams. The final result we obtain is valid for an arbitrary relative phase η which goes beyond the result obtained by Wabnig *et al.* in Ref. 18. This fact allows us to study the p detector in fourth-order perturbation theory.

1. Results for $\hat{S}_D^{(4)}(\tau_3, \tau_4)$, $\check{S}_D^{(4)}(\tau_3, \tau_4)$, $\hat{S}_{DD}^{(4)}(\tau_3, \tau_4)$, and $\check{S}_{DD}^{(4)}(\tau_3, \tau_4)$

In the following, we sum up the different types of diagrams, bubble-type diagrams as well as closed-loop diagrams; both then can be integrated exactly.

First we consider all diagrams containing only one oscillator line; these diagrams are all proportional to $t_0^2 t_1^2$ and depend on η . We find for the symmetrized frequency-dependent current noise

$$\hat{S}_{\text{sym,D}}^{(4)}(\omega) = 4\pi^2 e^2 \rho_0^4 t_0^2 t_1^2 \left\{ \cos(\eta)^2 \times \left[4e^2 V^2 - 4eV\sigma^-(\omega, V) \frac{Q(\omega)}{S_x(\omega)} \right] S_x(\omega) \right.$$

$$\left. + \sin(\eta)^2 \left[\omega^2 - 2\omega\sigma^+(\omega, V) \frac{Q(\omega)}{S_x(\omega)} \right] S_x(\omega) + \frac{1}{2} [D^R(\omega) + D^A(\omega)] \cos(\eta) \sin(\eta) \times [4eV\sigma^+(\omega, V) - 2\omega\sigma^-(\omega, V)] \right\}, \quad (52)$$

which is one of the main results of this paper.

In the case of the closed-loop diagrams containing one oscillator line, it is also possible to sum up all diagrams and integrate them exactly. The expression for $\check{S}_{\text{sym,D}}^{(4)}(\omega)$ is rather lengthy therefore we do not present it here.

We find that the current noise signature of $\check{S}_{\text{sym,D}}^{(4)}(\omega)$ is of the kinklike structure similar to $S_{\text{sym,D}}^{(2)}(\omega)$. In addition to the kinks at $|\omega| = |V \pm \Omega|$ coming from $S_{\text{sym,D}}^{(2)}(\omega)$, $\check{S}_{\text{sym,D}}^{(4)}(\omega)$ gives rise to extra kinks at $|\omega| = |V|$ and $|\omega| = |\Omega|$. However, these contributions are only minor modifications to the current noise floor $S_{\text{sym,D}}^{(2)}(\omega)$. Experiments as in Ref. 20 focus on the current noise near the resonance frequency $\omega \approx \Omega$ for which $\hat{S}_{\text{sym,D}}^{(4)}(\omega)$ is the most important contribution. Therefore the discussion of our result will focus on the contributions stemming from

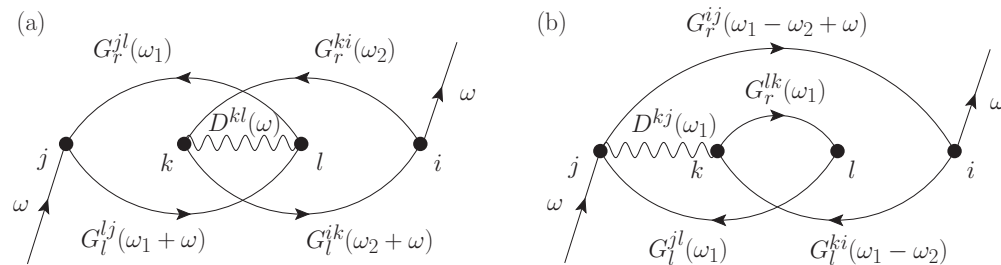


FIG. 4. Examples of diagrams containing one oscillator correlation function D . In panel (a) a bubble diagram is depicted where the oscillator line is independent of an internal frequency. Panel (b) shows a closed-loop diagram where the oscillator line always appears under integration of an internal frequency.

$\hat{S}_{\text{sym,D}}^{(4)}(\omega)$. These contributions possess a peaked structure, since the oscillator correlation functions $D^{R/A}(\omega)$ and the spectrum $S_x(\omega)$ is peaked around $\omega = \pm\Omega$.

The other contributions to the current noise stem from diagrams containing two oscillator lines $D(t, t')$. These diagrams are all proportional to $\beta_1 \beta_1^* \beta_1 \beta_1^* = t_1^4$ and therefore independent of the relative phase η between t_0 and t_1 . Moreover, these current noise contributions are small compared to the ones containing only one oscillator line since $t_1^4 \ll t_0^2 t_1^2$. We, however, are mainly interested in the possibility to detect the oscillator's momentum, which depends on η ; for this reason and the fact that they are small compared to $\hat{S}_{\text{sym,D}}^{(4)}(\omega)$ we do not include them in our discussion, nevertheless we state our result, which we obtain after summing up the diagrams

$$\begin{aligned} \hat{S}_{DD}^{(4)ij}(\omega) = & -\frac{e^2}{2\pi} \int d\omega_1 \sum_{k,l=\pm} (kl) \{ D^{kl}(\omega_1) \\ & \times D^{ij}(\omega_1 + \omega) \bar{G}_{11}^{kj}(-\omega_1) \bar{G}_{11}^{li}(\omega_1) \\ & + D^{ki}(\omega_1) D^{lj}(\omega_1 + \omega) \bar{G}_{11}^{kj}(-\omega_1) \bar{G}_{11}^{li}(-\omega_1 - \omega) \\ & - D^{ki}(\omega_1) D^{lj}(-\omega_1) \mathcal{G}_{11}^{kl}(-\omega_1) \mathcal{G}_{11}^{ij}(\omega_1 + \omega) \}. \end{aligned} \quad (53)$$

The last integration in Eq. (53) can be easily done since the oscillator correlation functions are peaked at $\pm\Omega$. Our result is then in accordance with the one obtained by Wabnig *et al.* in Ref. 18, where it has been shown that these contributions to the current noise are peaked at $\omega = -2\Omega, 0, 2\Omega$ in contrast to the contributions arising from Eq. (52). Similar to $\check{S}_D^{(4)}(\omega)$, $\check{S}_{DD}^{(4)}(\omega)$ is of the kinklike structure and therefore only modifying the current noise floor. We now address the current noise stemming from $\hat{S}_{\text{sym,D}}^{(4)}(\omega)$ for arbitrary η and also arbitrary system parameters.

2. Current noise in the Markovian and non-Markovian regime for arbitrary η

In order to compare our result for the momentum detector with Ref. 17, we investigate $\hat{S}_{\text{sym,D}}^{(4)}(\omega)$ near the resonance ($\omega \approx \Omega$). We find

$$\begin{aligned} \hat{S}_{\text{sym,D}}^{(4)}(\omega) \approx & 4\pi^2 e^2 \rho_0^4 t_0^2 t_1^2 \left\{ 4e^2 V^2 \cos(\eta)^2 \right. \\ & \times \left[1 - \frac{\sigma^-(\Omega, V)}{4eVm\Omega \langle \bar{x}^2 \rangle} \sqrt{1 - \left(\frac{\gamma_{\text{tot}}}{\Omega} \right)^2} \right] S_x(\omega) \\ & + \frac{1}{m^2} \sin(\eta)^2 \left[1 - \frac{2\sigma^+(\Omega, V)m}{\langle \bar{p}^2 \rangle} \right. \\ & \times \sqrt{1 - \left(\frac{\gamma_{\text{tot}}}{\Omega} \right)^2} \left. \right] S_p(\omega) \\ & + \cos(\eta) \sin(\eta) \frac{1}{m} \frac{\omega^2 - \Omega^2}{4\gamma_{\text{tot}}^2 \Omega^2 + (\omega^2 - \Omega^2)^2} \\ & \left. \times [4eV\sigma^+(\Omega, V) - 2\Omega\sigma^-(\Omega, V)] \right\}, \end{aligned} \quad (54)$$

where $\sigma^\pm(\xi, V)$ is given in Eq. (42) and $S_x(\omega)$ and $S_p(\omega)$ near resonance are given by

$$S_X(\omega) = \frac{2\gamma_{\text{tot}}^2 \Omega^2 \langle \bar{X}^2 \rangle}{4\gamma_{\text{tot}}^2 \Omega^2 + (\omega^2 - \Omega^2)^2}, \quad (55)$$

with $X = x, p$. The above expression is valid for the Markovian as well as for the non-Markovian regime. The relevant information about the oscillator can now be gained from the current noise spectrum.

We take two different ways of evaluating the expectation values $\langle \bar{x}^2 \rangle$ and $\langle \bar{p}^2 \rangle$. In the first one we use number states which lead to expectation values $\langle \bar{x}^2 \rangle_n = (2n + 1)/m\Omega$ and $\langle \bar{p}^2 \rangle_n = (2n + 1)m\Omega$, where n denotes the oscillator's number of quanta.

Since we also could imagine, as already explained in Sec. IV B 1, two equilibrium baths, the tunnel junction and an external heat bath, to which the oscillator couples, we can assign an effective temperature T_{eff} to the oscillator which obeys $\gamma_{\text{tot}} T_{\text{eff}} = \gamma_0 T_{\text{env}} + \gamma_+ T_{\text{junc}}$, where $\gamma_{\text{tot}} = \gamma_0 + \gamma_+$ is the total damping due to coupling to the junction (γ_+) and an external heat bath (γ_0). The external heat bath is at temperature T_{env} and the junction's temperature is given by $T_{\text{junc}} = eV/2k_B$. The oscillator's expectation values in this thermal regime are then given by $\langle \bar{x}^2 \rangle = 2k_B T_{\text{eff}}/m\Omega^2$ and $\langle \bar{p}^2 \rangle = 2mk_B T_{\text{eff}}$.

For both cases, the thermal state and the number state one, it is convenient scaling the current noise $\hat{S}_{\text{sym,D}}^{(4)}(\omega)$ with $eI_0 = 2\pi\rho_0^2 e^2 t_0^2 \sigma^+(\Omega, V)$. We furthermore introduce dimensionless constant f_1, f_2, f_3, f_4 which are defined in the following way:

$$\gamma_{\text{tot}} = \frac{\Omega}{f_1}, \quad (56)$$

$$\gamma_+ = \frac{\gamma_{\text{tot}}}{f_2} = \frac{\Omega}{f_1 f_2}, \quad (57)$$

$$eV = f_3 \Omega, \quad (58)$$

$$T_{\text{env}} = f_4 \frac{eV}{k_B}. \quad (59)$$

f_1 can be interpreted as an overall quality factor. The ratio $\gamma_0/\gamma_+ = (f_2 - 1)$ leads for $f_2 \in]1, 2[$ to a stronger coupling to the tunnel junction and for $f_2 > 2$ to a stronger coupling to the external heat bath. The parameter f_3 distinguishes the non-Markovian ($f_3 \in]0, 1[$) from the Markovian regime ($f_3 \gg 1$). The last parameter f_4 quantifies the temperature T_{env} of the external bath with respect to the applied bias V .

We now compare the signal of the position detector $S_{x\text{-det}}^{(4)}(\omega) = \hat{S}_{\text{sym,D}}^{(4)}(\omega; \eta = 0)$ to the signal of the momentum detector $S_{p\text{-det}}^{(4)}(\omega) = \hat{S}_{\text{sym,D}}^{(4)}(\omega; \eta = \pi/2)$ and later their dependencies on the parameters f_i at resonance $\omega \approx \Omega$. Assuming a high quality resonator we take $\sqrt{1 - \gamma_{\text{tot}}^2/\Omega^2} \approx 1$ in Eq. (54). We call $\mathcal{Q}_x = \sigma^-(\Omega, V)/(4eVm\Omega \langle \bar{x}^2 \rangle)$ quantum corrections to the x -detector current noise, arising from the nonvanishing commutator $[\hat{x}, \hat{p}]$; similarly we call $\mathcal{Q}_p = [2m\sigma^+(\Omega, V)]/\langle \bar{p}^2 \rangle$ quantum corrections to the p -detector current noise. We then find

$$S_{x\text{-det}}^{(4)} = 4f_3^2 \frac{[1 - \mathcal{Q}_x]}{[1 - \mathcal{Q}_p]} S_{p\text{-det}}^{(4)} \quad (60)$$

and conclude that in the Markovian regime where $f_3 \gg 1$ the signal of the position detector is always larger than the signal of the momentum detector, whereas in the non-Markovian regime we have a stronger signature of the noise part showing the momentum signature of the oscillator. In the following, we investigate in more detail the current noise of the x and p detector.

3. The x detector

From Eq. (54) one can see that for $\eta = 0 \bmod \pi$ we recover the position-detector result as in Refs. 14, 16, and 18, with peaks in the current noise spectrum at $\omega = \pm\Omega$. Since we calculate the symmetrized current-current correlator, the current noise is symmetric in ω . The sign of the signal is given by the sign of $[1 - \mathcal{Q}_x]$, which for an oscillator in number state n it depends on n and f_3 only. We stick to a thermal resonator, noting that as in Ref. 17 for the p detector, here the quantum corrections $\mathcal{Q}_x \sim 1/f_3$ can become large (compared to 1) in the non-Markovian regime where $f_3 < 1$, leading to a sign change. The parameter regimes for a negative/positive peak in the current noise are depicted in Fig. 5 as blue/red regions. The change of sign in the signal depends on the environment temperature T_{env} , the coupling to the environments f_2 , and heavily on the bias voltage and therefore f_3 . Deep in the Markovian regime the sign change is hard to achieve, only if f_2 is very large and the bath temperature T_{env} is very low, meaning that heating of the oscillator can be compensated by strongly coupling to a cold environment. In the non-Markovian regime the quantum corrections \mathcal{Q}_x can become

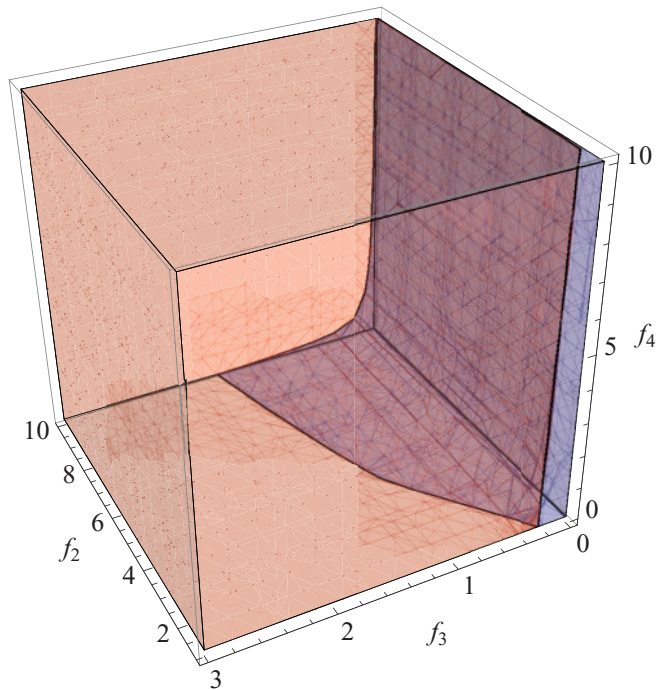


FIG. 5. (Color online) The current noise peak at $\omega = \Omega$ for the x detector as a function of f_2, f_3, f_4 , where we took $f_1 \rightarrow \infty$. The blue region shows the parameter regime where the peak is negative, for parameter combinations lying in the red region, the peak is positive.

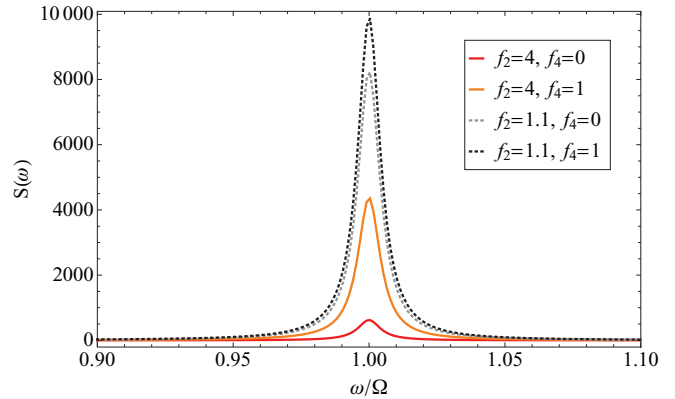


FIG. 6. (Color online) Noise signal at $\omega = \Omega$ in the Markovian regime for different values of f_2 and f_4 with $f_1 = 200$ and $f_3 = 50$, which shows a peak due to the presence of the oscillator. The noise is scaled by $2\pi\rho_0^2 e^2 t_0^2 \sigma^+(\Omega, V)$.

large more easily and due to the lower signal in the non-Markovian regime for the x detector, the sign change is more pronounced.

Figures 6 and 7 show the current noise spectrum around $\omega \approx \Omega$ in the Markovian and the non-Markovian regime for different couplings and environment temperatures.

4. The p detector

For the cases $\eta = \pi/2 \bmod \pi$ in Eq. (54), the result of the momentum detector as stated in Ref. 17 are extended to the non-Markovian regime. Due to the fact that the quantum corrections \mathcal{Q}_p are in the first place larger than \mathcal{Q}_x , the peak in the current noise spectrum stemming from the oscillator has a negative sign for $\eta = \pi/2$. However, it is also possible to change the sign by adjusting the parameters f_2, f_3, f_4 on which \mathcal{Q}_p depends. In Fig. 8 we depict the regions with a negative sign blue and the ones with a positive sign red. Changing the sign of the current noise signal in the p -detector case is easier

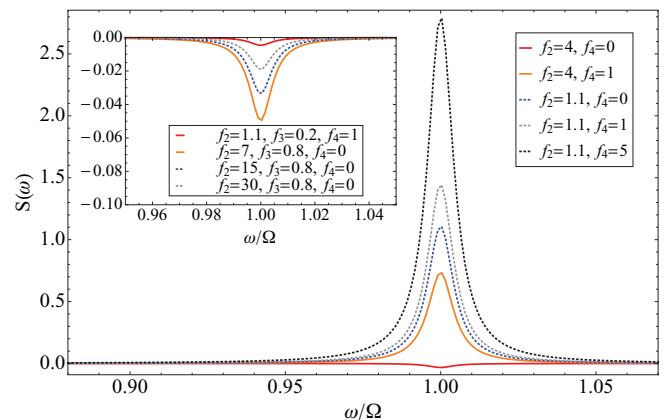


FIG. 7. (Color online) x -detector current noise signal [scaled by $2\pi\rho_0^2 e^2 t_0^2 \sigma^+(\Omega, V)$] at $\omega = \Omega$ in the non-Markovian regime for different values of f_2 and f_4 with $f_1 = 200$ and $f_3 = 0.8$. We note that the signal is weaker than in the Markovian regime (compare to Fig. 6). In this regime, however, it is possible to see a change of sign of the signal, depending on the parameters f_2, f_4 . The inset illustrates this sign change.

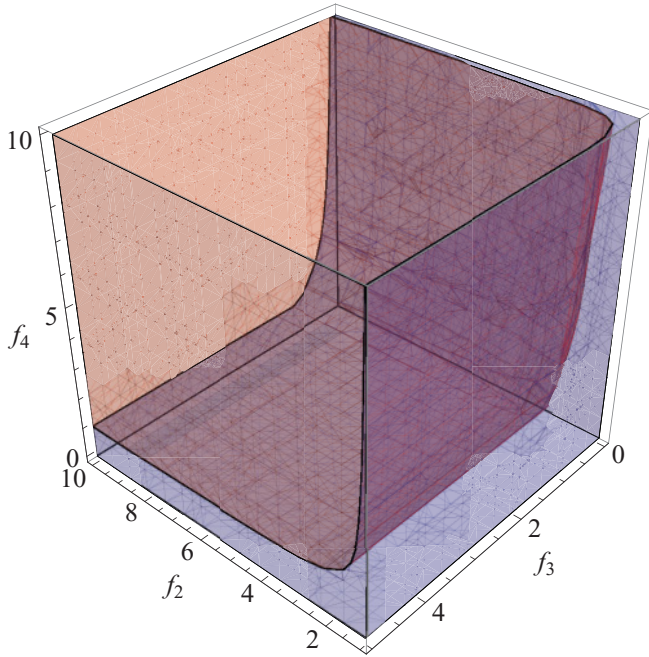


FIG. 8. (Color online) This figure shows the parameter regimes for the p detector where the current noise peak at $\omega = \Omega$ has a negative sign (blue) and positive sign (red). Compared to the x detector the sign change is possible for a wider range of parameters f_2, f_3, f_4 ; we took $f_1 \rightarrow \infty$.

to achieve over a wide range of parameters, as compared to the x detector, even deep in the Markovian regime ($f_3 \gg 1$). Figure 9 shows a summary of the p -detector current noise in the Markovian and non-Markovian regimes for different parameters f_2, f_4 , respectively.

5. Detection of number states

With the expression for the current noise and definitions above it is possible to determine the occupation number of the

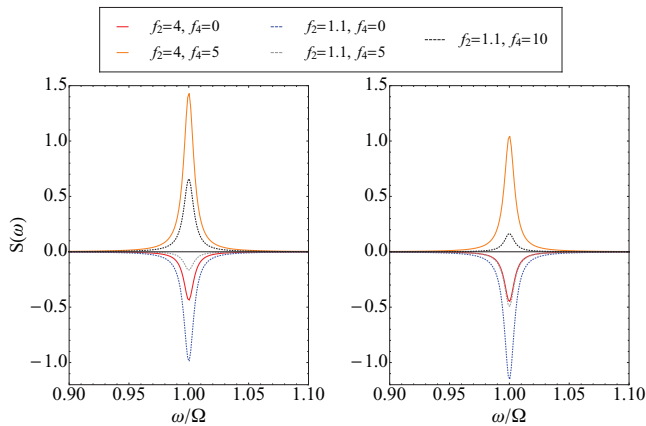


FIG. 9. (Color online) The left panel shows the p -detector current noise [scaled by $2\pi\rho_0^2 e^2 t_0^2 \sigma^+(\Omega, V)$] in the Markovian regime ($f_3 = 50$) for various parameters f_2, f_4 , and $f_1 = 200$. The right panel shows the current noise in the non-Markovian regime ($f_3 = 0.8$) for various parameters f_2, f_4 . In both cases we can easily achieve a sign change in the signal.

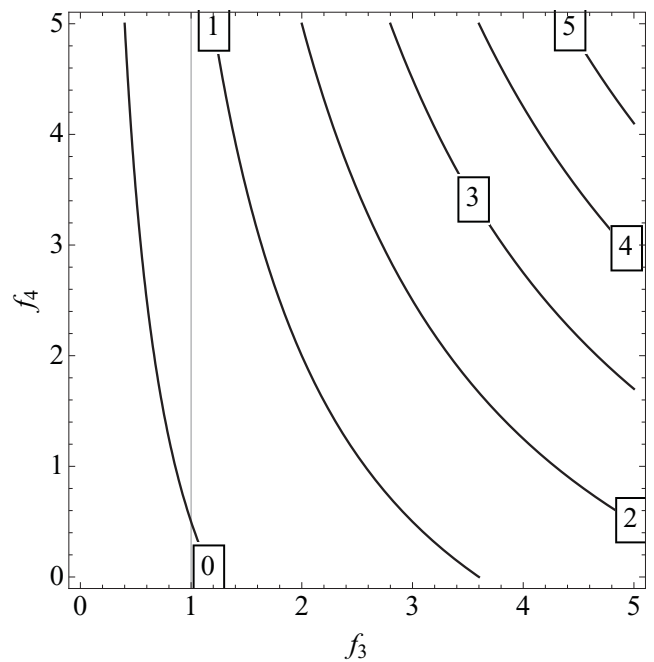
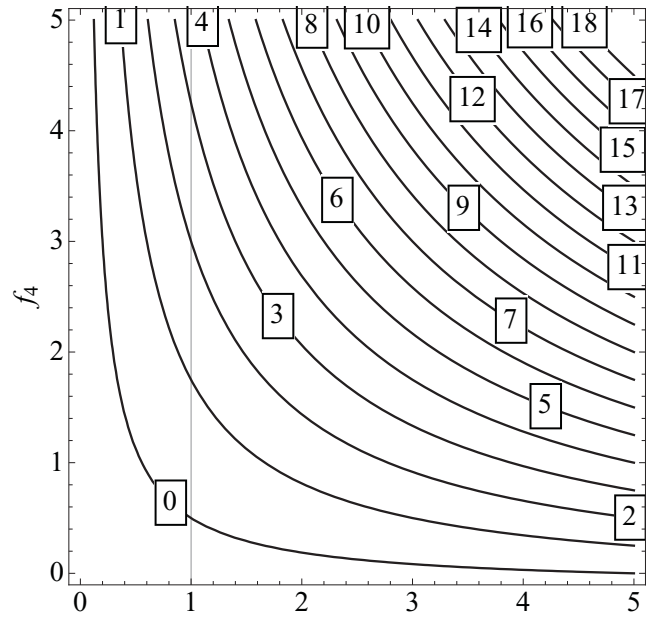


FIG. 10. Number of quanta n on the oscillator in dependence of experimentally adjustable parameters, for dominant coupling to the external heat bath (upper panel, with $f_2 = 5$) and dominant coupling to the tunnel junction (lower panel, with $f_2 = 1.2$).

oscillator, in similar fashion to Ref. 18. Equation (54) for the current noise contains position and momentum expectation values of the oscillator which can be evaluated using (i) number states and (ii) a thermal state. In the case of number states the gained expression depends on n , the number of quanta on the oscillator, whereas in the case of a thermal state, it depends on the experimentally adjustable parameters f_i . Arguing that the current noise signal is the same if

$\langle X \rangle_n = \langle X \rangle_{\text{th}}$, leads to the following dependence of n on the parameters f_i :

$$n = \frac{2f_2|f_3|f_4 - 2|f_3|f_4 - f_2 + |f_3|}{2f_2}. \quad (61)$$

The dependence of n on the adjustable parameters is depicted in Fig. 10, where for specific values of f_3 and f_4 , which can be experimentally adjusted, and fixed values of f_1 and f_2 , the contour lines show the corresponding number state. In principle, this can serve as a guidance for experimentalists to put the oscillator in a given number state. By a later noise measurement it could be verified whether the data are consistent with this specific number state. Moreover, we can in principle fully determine the state of the oscillator via its covariance matrix σ by two noise measurements (one with $\eta = 0$ and one where $\eta = \pi/2$) which adds a second possibility to verify whether Eq. (61) serves as a good guide. Figure 10 shows that in the Markovian regime the oscillator is only in its ground state for low environmental temperatures, since the applied bias voltage is heating the oscillator. In the non-Markovian regime, we can have a higher environmental temperature for the oscillator being in its ground state.

VI. CONCLUSION

We have studied the finite frequency current noise of a tunnel junction coupled to a harmonic oscillator. In our work, we go beyond the Born approximation (because we calculate the noise up to fourth order in the tunneling amplitude) and beyond the Markov approximation (because we do not restrict ourselves to the regime $eV/\hbar\Omega \gg 1$). For a nonstationary oscillator, we have shown that the finite frequency current noise of the detector can be complex. This complex current noise can be used to obtain information about expectation values depending on \hat{x} as well as expectation values depending on \hat{p} . The former we call the x -detector signal and the latter the p -detector signal.

For the stationary oscillator, the finite frequency current noise is always real. Then, it is more complicated to get momentum information using a tunnel junction detector. An Aharonov-Bohm-loop setup is needed for this task. We analyze such a setup for the first time in the non-Markovian regime and thereby show how the x and the p signals can be used to determine the quantum state of the oscillator.

Our analysis is an essential prerequisite to study how the quantum entanglement of NEMS (Ref. 32) can be measured on the basis of tunnel junction detectors. This very interesting problem will be addressed in future work.

ACKNOWLEDGMENTS

We thank T. L. Schmidt and K. Børkje for interesting discussions and acknowledge financial support from the DFG.

APPENDIX A: DETAILS ON THE FERMIONIC GREEN'S FUNCTIONS

Expectation values of the fermionic operators \hat{h}_i and \hat{j}_i can be expressed by the Keldysh Green's functions $G_{l,r}(t, t') = -i \langle T_c \hat{c}_{l,r}(t) \hat{c}_{l,r}^\dagger(t') \rangle$ as

$$\begin{aligned} \langle T_c \hat{h}_i(t) \hat{j}_j(t') \rangle &= -i \bar{\mathcal{G}}_{ij}(t, t') \\ &= -i [\beta_i \beta_j^* G_r(t, t') G_l(t', t) \\ &\quad - \beta_i^* \beta_j G_r(t', t) G_l(t, t')], \end{aligned} \quad (A1)$$

$$\begin{aligned} \langle T_c \hat{h}_i(t) \hat{h}_j(t') \rangle &= \mathcal{G}_{ij}(t, t') \\ &= [\beta_i \beta_j^* G_r(t, t') G_l(t', t) \\ &\quad + \beta_i^* \beta_j G_r(t', t) G_l(t, t')], \end{aligned} \quad (A2)$$

$$\begin{aligned} \langle T_c \hat{j}_i(t) \hat{j}_j(t') \rangle &= \mathcal{G}_{ij}(t, t') \\ &= [\beta_i \beta_j^* G_r(t, t') G_l(t', t) \\ &\quad + \beta_i^* \beta_j G_r(t', t) G_l(t, t')]. \end{aligned} \quad (A3)$$

The Fourier transform of the function $\mathcal{G}_{ij}(t, t')$ can be calculated in the usual way, yielding

$$\begin{aligned} \mathcal{G}_{ij}^+(\omega)^+ &= 2\pi\rho_0^2 \left\{ \beta_i \beta_j^* \frac{eV + \omega}{2} \left[-1 + \coth\left(\beta \frac{eV + \omega}{2}\right) \right] \right. \\ &\quad \left. + \beta_i^* \beta_j \frac{eV - \omega}{2} \left[1 + \coth\left(\beta \frac{eV - \omega}{2}\right) \right] \right\}, \end{aligned} \quad (A4)$$

$$\begin{aligned} \mathcal{G}_{ij}^+(\omega)^+ &= 2\pi\rho_0^2 \left\{ \beta_i \beta_j^* \frac{eV + \omega}{2} \left[1 + \coth\left(\beta \frac{eV + \omega}{2}\right) \right] \right. \\ &\quad \left. + \beta_i^* \beta_j \frac{eV - \omega}{2} \left[-1 + \coth\left(\beta \frac{eV - \omega}{2}\right) \right] \right\}, \end{aligned} \quad (A5)$$

$$\begin{aligned} \bar{\mathcal{G}}_{ii}^-(\omega) &= \bar{\mathcal{G}}_{ii}^{++}(\omega) \\ &= \beta_i \beta_i^* \int \frac{d\omega_1}{2\pi} [G_r^{--}(\omega_1 + \omega) G_l^{--}(\omega_1) \\ &\quad - G_r^{--}(\omega_1) G_l^{--}(\omega_1 + \omega)] \\ &= 2\pi\rho_0^2 \beta_i \beta_i^* \sigma^-(\omega, V), \end{aligned} \quad (A6)$$

where $\sigma^-(\omega, V)$ is given in Eq. (42).

APPENDIX B: DETAILS OF THE SECOND-ORDER CURRENT NOISE CALCULATION

The starting point for the calculation is Eq. (40); together with Eqs. (11) and (12) the symmetrized current noise in the nonstationary case can be written as

$$\begin{aligned} S_{\text{sym}}^{(2)}(\omega, t') &= \frac{e^2}{2} \int dt e^{i\omega t} \left\{ \mathcal{G}_{00}^{--}(t) + \mathcal{G}_{00}^{++}(t) \right. \\ &\quad \left. + \langle \hat{x}(t') \rangle [\mathcal{G}_{01}^{--}(t) + \mathcal{G}_{01}^{++}(t)] + \langle \hat{x}(t') \rangle \cos(\Omega t) \right. \\ &\quad \left. \times [\mathcal{G}_{10}^{--}(t) + \mathcal{G}_{10}^{++}(t)] + \frac{\langle \hat{p}(t') \rangle}{m\Omega} \right. \\ &\quad \left. \times \sin(\Omega t) [\mathcal{G}_{10}^{--}(t) + \mathcal{G}_{10}^{++}(t)] \right. \\ &\quad \left. + \langle \hat{x}(t') \hat{x}(t') \rangle \cos(\Omega t) [\mathcal{G}_{11}^{--}(t) + \mathcal{G}_{11}^{++}(t)] \right\} \end{aligned}$$

$$+ \frac{\langle \hat{x}(t') \hat{p}(t') \rangle}{m\Omega} \sin(\Omega t) \mathcal{G}_{11}^{-+}(t) \\ + \frac{\langle \hat{p}(t') \hat{x}(t') \rangle}{m\Omega} \sin(\Omega t) \mathcal{G}_{11}^{+-}(t) \Big\}. \quad (\text{B1})$$

Further calculation is straightforward by using Eqs. (A4) and (A5). Finally, the current noise $S_{\text{sym}}^{(2)}(\omega, t')$ in Eq. (B1) can be written as

$$S_{\text{sym}}^{(2)}(\omega, t') = \frac{e^2}{2} \left\{ \mathcal{G}_{00}^{-+}(\omega) + \mathcal{G}_{00}^{+-}(\omega) + \langle \hat{x}(t') \rangle \right. \\ \times [\mathcal{G}_{01}^{-+}(\omega) + \mathcal{G}_{01}^{+-}(\omega)] + \frac{1}{2} \langle \hat{x}(t') \rangle [\mathcal{G}_{10}^{-+}(\omega + \Omega) \\ + \mathcal{G}_{10}^{-+}(\omega - \Omega) + \mathcal{G}_{10}^{+-}(\omega + \Omega) + \mathcal{G}_{10}^{+-}(\omega - \Omega)] \\ - \frac{i}{2m\Omega} \langle \hat{p}(t') \rangle [\mathcal{G}_{10}^{-+}(\omega + \Omega) - \mathcal{G}_{10}^{-+}(\omega - \Omega) \\ + \mathcal{G}_{10}^{+-}(\omega + \Omega) - \mathcal{G}_{10}^{+-}(\omega - \Omega)] + \frac{1}{2} \langle \hat{x}(t') \hat{x}(t') \rangle \\ \times [\mathcal{G}_{11}^{-+}(\omega + \Omega) + \mathcal{G}_{11}^{-+}(\omega - \Omega) + \mathcal{G}_{11}^{+-}(\omega + \Omega) \\ + \mathcal{G}_{11}^{+-}(\omega - \Omega)] - \frac{i}{2m\Omega} \langle \hat{x}(t') \hat{p}(t') \rangle \\ \times [\mathcal{G}_{11}^{-+}(\omega + \Omega) - \mathcal{G}_{11}^{-+}(\omega - \Omega)] \\ - \frac{i}{2m\Omega} \langle \hat{p}(t') \hat{x}(t') \rangle \\ \left. \times [\mathcal{G}_{11}^{+-}(\omega + \Omega) - \mathcal{G}_{11}^{+-}(\omega - \Omega)] \right\}. \quad (\text{B2})$$

The functions $\sigma^\pm(\xi, V)$, see Eq. (42), allow us to distinguish the Markovian from the non-Markovian regime. For $T \rightarrow 0$ we find

$$\sigma^-(\xi, V) = \begin{cases} \text{sgn}(V) \xi & e|V| > \xi \\ \text{sgn}(V) e|V| & e|V| < \xi \end{cases}, \quad (\text{B3})$$

$$\sigma^+(\xi, V) = \begin{cases} e|V| & e|V| > \xi \\ \xi & e|V| < \xi \end{cases}, \quad (\text{B4})$$

where T here is the temperature of electrons in the leads.

APPENDIX C: DETAILS OF THE FOURTH-ORDER CURRENT NOISE CALCULATION

We first give the whole expression for the current noise to fourth order in the tunneling amplitudes containing the \mathcal{M} functions of Eq. (49) and oscillator operators

$$S^{(4)}(\tau_3, \tau_4) \\ = -\frac{e^2}{2} \int_c d\tau_1 d\tau_2 \{ \mathcal{M}_{0,0,0,0}(\tau_1, \tau_2, \tau_3, \tau_4) \\ + \mathcal{M}_{0,0,0,1}(\tau_1, \tau_2, \tau_3, \tau_4) \langle \hat{x}(\tau_4) \rangle \\ + \mathcal{M}_{0,0,1,0}(\tau_1, \tau_2, \tau_3, \tau_4) \langle \hat{x}(\tau_3) \rangle \\ + \mathcal{M}_{0,1,0,0}(\tau_1, \tau_2, \tau_3, \tau_4) \langle \hat{x}(\tau_2) \rangle \\ + \mathcal{M}_{1,0,0,0}(\tau_1, \tau_2, \tau_3, \tau_4) \langle \hat{x}(\tau_1) \rangle \\ + \mathcal{M}_{0,0,1,1}(\tau_1, \tau_2, \tau_3, \tau_4) \langle T_c \hat{x}(\tau_3) \hat{x}(\tau_4) \rangle \\ + \mathcal{M}_{0,1,0,1}(\tau_1, \tau_2, \tau_3, \tau_4) \langle T_c \hat{x}(\tau_2) \hat{x}(\tau_4) \rangle \\ + \mathcal{M}_{0,1,1,0}(\tau_1, \tau_2, \tau_3, \tau_4) \langle T_c \hat{x}(\tau_2) \hat{x}(\tau_3) \rangle \\ + \mathcal{M}_{1,0,0,1}(\tau_1, \tau_2, \tau_3, \tau_4) \langle T_c \hat{x}(\tau_1) \hat{x}(\tau_4) \rangle \\ + \mathcal{M}_{1,0,1,0}(\tau_1, \tau_2, \tau_3, \tau_4) \langle T_c \hat{x}(\tau_1) \hat{x}(\tau_3) \rangle \\ + \mathcal{M}_{1,1,0,0}(\tau_1, \tau_2, \tau_3, \tau_4) \langle T_c \hat{x}(\tau_1) \hat{x}(\tau_2) \rangle \\ + \mathcal{M}_{0,1,1,1}(\tau_1, \tau_2, \tau_3, \tau_4) \langle T_c \hat{x}(\tau_2) \hat{x}(\tau_3) \hat{x}(\tau_4) \rangle \\ + \mathcal{M}_{1,0,1,1}(\tau_1, \tau_2, \tau_3, \tau_4) \langle T_c \hat{x}(\tau_1) \hat{x}(\tau_3) \hat{x}(\tau_4) \rangle \\ + \mathcal{M}_{1,1,0,1}(\tau_1, \tau_2, \tau_3, \tau_4) \langle T_c \hat{x}(\tau_1) \hat{x}(\tau_2) \hat{x}(\tau_4) \rangle \\ + \mathcal{M}_{1,1,1,0}(\tau_1, \tau_2, \tau_3, \tau_4) \langle T_c \hat{x}(\tau_1) \hat{x}(\tau_2) \hat{x}(\tau_3) \rangle \\ + \mathcal{M}_{1,1,1,1}(\tau_1, \tau_2, \tau_3, \tau_4) \langle T_c \hat{x}(\tau_1) \hat{x}(\tau_2) \hat{x}(\tau_3) \hat{x}(\tau_4) \rangle \} \\ + \int_c d\tau_1 d\tau_2 \langle T_c \hat{H}_{\text{tun}}(\tau_1) \hat{I}(\tau_3) \rangle \langle T_c \hat{H}_{\text{tun}}(\tau_2) \hat{I}(\tau_4) \rangle. \quad (\text{C1})$$

A first reduction of terms in Eq. (C1) is done by only focusing on the stationary case. This allows us to drop terms which are proportional to $\langle \hat{x}(t) \rangle$ of Eq. (C1) and only keep terms proportional to $D(t, t')$ and $D(t, t') D(t'', t''')$. Unlinked diagrams which appear in this expression are canceled by the \hat{I}^2 term, which is always of the bubble type.

¹K. Schwab and M. Roukes, *Phys. Today* **58**(7), 36 (2005).

²A. A. Clerk, S. M. Girvin, F. Marquardt, and R. J. Schoelkopf, *Rev. Mod. Phys.* **82**, 1155 (2010).

³Y. Yang, C. Callegari, X. Feng, K. Ekinici, and M. Roukes, *Nano Lett.* **6**, 583 (2006).

⁴H. Mamin and D. Rugar, *Appl. Phys. Lett.* **79**, 3358 (2001).

⁵M. LaHaye, O. Buu, B. Camarota, and K. Schwab, *Science* **304**, 74 (2004).

⁶B. Lassagne, Y. Tarakanov, J. Kinaret, D. Garcia-Sanchez, and A. Bachtold, *Science* **325**, 1107 (2009).

⁷G. A. Steele, A. K. Huttel, B. Witkamp, M. Poot, H. B. Meerwaldt, L. P. Kouwenhoven, and H. S. J. van der Zant, *Science* **325**, 1103 (2009).

⁸M. Hofheinz, H. Wang, M. Ansmann, R. Bialczak, E. Lucero, M. Neeley, A. O'Connell, D. Sank, J. Wenner, and J. Martinis, *Nature (London)* **459**, 546 (2009).

⁹A. D. O'Connell *et al.*, *Nature (London)* **464**, 697 (2010).

¹⁰F. Marquardt, J. P. Chen, A. A. Clerk, and S. M. Girvin, *Phys. Rev. Lett.* **99**, 093902 (2007).

¹¹I. Wilson-Rae, N. Nooshi, W. Zwerger, and T. J. Kippenberg, *Phys. Rev. Lett.* **99**, 093901 (2007).

¹²T. Rocheleau, T. Ndukum, C. Macklin, J. B. Hertzberg, A. A. Clerk, and K. C. Schwab, *Nature (London)* **463**, 72 (2010).

¹³A. Naik, O. Buu, M. D. Lahaye, A. D. Armour, A. A. Clerk, M. P. Blencowe, and K. C. Schwab, *Nature (London)* **443**, 193 (2006).

¹⁴A. A. Clerk and S. M. Girvin, *Phys. Rev. B* **70**, 121303 (2004).

¹⁵J. Wabnig, D. V. Khomitsky, J. Rammer, and A. L. Shelankov, *Phys. Rev. B* **72**, 165347 (2005).

¹⁶C. B. Doiron, B. Trauzettel, and C. Bruder, *Phys. Rev. B* **76**, 195312 (2007).

¹⁷C. B. Doiron, B. Trauzettel, and C. Bruder, *Phys. Rev. Lett.* **100**, 027202 (2008).

- ¹⁸J. Wabnig, J. Rammer, and A. L. Shelankov, *Phys. Rev. B* **75**, 205319 (2007).
- ¹⁹G. Rastelli, M. Houzet, and F. Pistolesi, *Europhys. Lett.* **89**, 57003 (2010).
- ²⁰N. E. Flowers-Jacobs, D. R. Schmidt, and K. W. Lehnert, *Phys. Rev. Lett.* **98**, 096804 (2007).
- ²¹T. L. Schmidt, K. Børkje, C. Bruder, and B. Trauzettel, *Phys. Rev. Lett.* **104**, 177205 (2010).
- ²²J. Rammer and H. Smith, *Rev. Mod. Phys.* **58**, 323 (1986).
- ²³J. Rammer, *Quantum Field Theory of Non-equilibrium States* (Cambridge University Press, Cambridge, 2007).
- ²⁴D. Mozyrsky and I. Martin, *Phys. Rev. Lett.* **89**, 018301 (2002).
- ²⁵A. A. Clerk, *Phys. Rev. B* **70**, 245306 (2004).
- ²⁶Y. Blanter and M. Büttiker, *Phys. Rep.* **336**, 1 (2000).
- ²⁷R. J. Schoelkopf, P. J. Burke, A. A. Kozhevnikov, D. E. Prober, and M. J. Rooks, *Phys. Rev. Lett.* **78**, 3370 (1997).
- ²⁸G. Lesovik and R. Loosen, *JETP Lett.* **65**, 295 (1997).
- ²⁹U. Gavish, Y. Levinson, and Y. Imry, *Phys. Rev. B* **62**, 10637 (2000).
- ³⁰L. DiCarlo, Y. Zhang, D. T. McClure, C. M. Marcus, L. N. Pfeiffer, and K. W. West, *Rev. Sci. Instrum.* **77**, 073906 (2006).
- ³¹P. Nozières, *Theory of Interacting Fermi Systems* (Westview Press, 1997).
- ³²J. Eisert, M. B. Plenio, S. Bose, and J. Hartley, *Phys. Rev. Lett.* **93**, 190402 (2004).